Recurrent Nephrotic Plasma Activates Pro-fibrotic Signalling Pathways Downstream of Protease-activated Receptor 1

Musleeha Chesor (mc17013@bristol.ac.uk)
University of Bristol https://orcid.org/0000-0002-4534-6895
Jack Tuffin
University of Bristol https://orcid.org/0000-0001-8405-2948
Carl May
Irene Ghobrial
Melissa Little
melissa.little@mcri.edu.au https://orcid.org/0000-0003-0380-2263
Gavin Welsh
University of Bristol https://orcid.org/0000-0002-2148-6658
Moin Saleem
University of Bristol https://orcid.org/0000-0002-9808-4518

Article

Keywords: Nephrotic Plasma, podocyte, GlomSpheres

Posted Date: January 12th, 2022

DOI: https://doi.org/10.21203/rs.3.rs-1226619/v1

Recurrent nephrotic plasma activates pro-fibrotic signalling pathways downstream of protease-activated receptor 1

Musleeha Chesor[1,2], Jack Tuffin[1], Carl J. May[1], Irene Ghobrial[3], Melissa H. Little[3,4], Moin A. Saleem[1*], Gavin I. Welsh[1*]

[1]Bristol Renal, Translational Health Sciences, Bristol Medical School, University of Bristol, Bristol, United Kingdom

[2]Faculty of Medicine, Princess of Naradhiwas University, Narathiwat, Thailand

[3]Murdoch Children's Research Institute, Flemington Rd, Melbourne, 3052, VIC, Australia

[4]Department of Pediatrics, Faculty of Medicine, Dentistry and Health Sciences, University of Melbourne, VIC, Australia

[*]co-senior authors

Correspondence: Moin Saleem or Gavin Welsh, Bristol Renal, Translational Health Sciences, Bristol Medical School, University of Bristol, Bristol, United Kingdom. E-mail: m.saleem@bristol.ac.uk or g.i.welsh@bristol.ac.uk

Abstract

Recurrence of steroid-resistant nephrotic syndrome (SRNS) is thought to be due to an unknown "circulating factor", the identity of which has so far remained elusive. Our previous work suggests a signaling role for protease-activated receptor-1 (PAR-1), leading to impaired podocyte function. Here, we show that relapse nephrotic plasma (NP), but not paired remission plasma, induced a pro-fibrotic response. This change was inhibited by PAR-1 inhibitors, but not by TGF-β1 inhibition. Four PAR-1 inhibitors demonstrated distinct antagonistic properties. The phosphorylation of VASP and JNK in a 3D spheroid model (GlomSpheres) and kidney organoids corroborated the finding from a 2D ciPods model. Functionally, relapse NP induced podocyte motility, and podocyte loss from spheroids both of which were also selectively rescued by PAR-1 inhibitors. Also, it induced the loss of

podocyte-specific markers in kidney organoids. We propose that the circulating factor acts as a pro-fibrotic effector by activating PAR-1, leading to increased podocyte injury.

Introduction

Idiopathic nephrotic syndrome (INS) arises from structural and functional alterations in the glomerular filtration barrier.[1] Currently, INS can be classified into two main groups; genetic, and immune-mediated, with a subset of the latter being circulating factor disease (CFD).[2] The classification of INS is also based on the response to steroid treatment as Steroid Sensitive Nephrotic Syndrome (SSNS) defined as achieving complete remission within four weeks after corticosteroid treatment, and Steroid Resistant Nephrotic Syndrome (SRNS) characterized by failure to respond to 4 weeks of steroid therapy.[3] Steroid Resistant Nephrotic Syndrome (SRNS) is a devastating disease which usually progresses to end-stage renal disease (ESRD) within ten years and requires transplantation.[4] Notably, the recurrence of SRNS after transplantation is a common complication reported in up to 50% of patients.[5] A circulating factor in plasma is thought to be key to the pathogenesis of post-transplantation disease recurrence, which is distinct from monogenic disease. CFD can be diminished by plasma exchange suggesting circulating factor(s) in plasma which directly target the podocyte and intersect with signalling pathways affected by single gene defects, thereby leading to changes in podocyte motility.[2,6]. To date, several candidates for this putative circulating factor(s) have been proposed. These include hemopexin, a plasma protease that has an active role in remodelling actin cytoskeleton in podocytes[7] and soluble urokinase plasminogen activator receptor (suPAR), a circulating factor that is raised in patients with primary and recurrent SRNS causing downstream effects on podocyte motility via integrin β3 in podocytes.[8] Podocyte signalling pathways directly activated in response to human disease plasma remain poorly defined. Previous work published by our group suggests that the

unknown circulating factor(s) in recurrent SRNS plasma signals to PAR-1, resulting in VASP phosphorylation and increased podocyte motility.[9] PAR-1 is one of four family members of transmembrane G-coupled receptors (GPCRs) activated by enzymatic cleavage of the N-terminus of the receptor that acts as a tethered ligand activation[10]. PAR-1 activation can be stimulated in two different ways. These include 1) canonical pathway – the cleavage of PAR-1 receptor at a canonical cleavage site (Arg41) by thrombin results in unmasking of the tethered ligand domain and initiates the signaling via G_q, G_i or $G_{12/13}$ or β-arrestin; or 2) non-canonical pathway – the cleavage of the receptor by proteases such as elastase, MMP1, and APC at distinct sites induces the activation of biased signaling pathways.[11–13] Activation of PAR-1 induces various signaling effectors important for inducing cell shape changes, adhesion molecule expression, secretion of vasoactive factors, cellular growth and motility.[10] We reported that human Th17 cells produce a soluble factor that activates the same signalling pathways as patient relapse plasma via the PAR-1 receptor and increases the motility of podocytes in vitro.[14] For this study we planned to further explore the effects downstream of this signalling cascade in podocytes. We hypothesized that circulating factor(s) in recurrent SRNS plasma initiate signalling pathways via PAR-1 that stimulate pro-fibrotic activation of podocytes. We investigated a set of novel signalling pathways upregulated by exposure of ciPods to the plasma of patients with SRNS. Furthermore, we utilized two models of the human glomerulus, GlomSpheres[15] and human kidney organoids[16], to directly evaluate the effects of nephrotic plasma on the signalling of podocyte and podocyte injury.

We found that relapse NP promotes the phosphorylation of proteins related to fibrotic processes via the PAR-1 receptor, which is selectively and effectively inhibited by PAR-1 antagonists. Furthermore, treatment of relapse NP to GlomSpheres and kidney organoids significantly induced the signalling to VASP, JNK, and proteins in the fibrosis pathway, which

is completely consistent with the finding on a ciPods 2D model. Functionally, we show an increase in podocyte motility in ciPods and podocyte loss from GlomSpheres in response to relapse NP, both of which were also selectively rescued by PAR-1 inhibitors. Interestingly, we demonstrate the loss of podocyte specific markers in stem cell-derived kidney organoids after treatment with relapse NP. We suggest that a circulating factor in nephrotic plasma could act as a pro-fibrotic mediator via PAR-1, leading to podocyte injury in nephrotic syndrome.

RESULTS

Nephrotic plasma induces the phosphorylation of proteins involved in fibrotic processes

The interaction of the JNK pathway with the TGF-β1/SMAD pathway can enhance the expression of pro-fibrotic and pro-inflammatory factors leading to fibrosis and inflammation in the kidney.[17] Activation of JNK can promote the phosphorylation of proteins involved in the pro-fibrotic responses including c-Jun, ATF-2, and SMAD-dependent pathway; SMAD2, and SMAD3, leading to fibrosis.[17,18] Therefore, the phosphorylation of proteins related to TGF-β1/SMAD pathway were examined to elucidate the possible pathways associated with nephrotic plasma-induced podocyte injury. ciPods were treated with relapse and paired-remission plasma from 11 patients. Relapse NP significantly increased the phosphorylation of VASP, JNK, and proteins involved in pro-fibrotic pathways; ATF-2, SMAD2, SMAD3, and c-Jun in podocytes compared to paired-remission plasma and untreated cells (Figure 1).

PAR-1 agonism and TGF-β1 induce the same pro-fibrotic signalling in podocytes

In order to align the observation of PAR-1 activation in response to nephrotic plasma with our current finding of pro-fibrotic pathway activation, we compared the effects of PAR-1 agonism, TGF- β1 stimulation and nephrotic plasma. The activation of both TGF- β1 and PAR-1 signalling pathways is involved in kidney fibrosis.[19] ciPods were treated with either 10 ng/mL TGF-β1 or 15 uM PAR-1 agonist peptide at different time points (5, 15, 30, 45, and 60

minutes). As shown in Figure 2, treatment of ciPods with either PAR-1 agonist peptide or TGF-β1 resulted in the rapid phosphorylation of VASP, JNK, ATF-2, c-Jun, SMAD2, and SMAD3 compared to untreated control, which mimicked the response to nephrotic plasma treatment as shown above. These increases were time-dependent, maximal at 15-30 minutes and then gradually declining to the basal level. Interestingly, PAR-1 agonist peptide induced the phosphorylation of c-Jun, SMAD2, and SMAD3 more rapidly than TGF-β1 with the peaks at 15 and 30 minutes, respectively (Figure 2).

PAR-1 antagonists inhibit nephrotic plasma induced signaling to VASP and the pro-fibrotic pathway

We then explored receptor agonism involved in this finding by inhibition of the PAR-1 receptor. To date, several PAR-1 targeting modulators have been developed including proteases, small molecules (SCH79797, FR171113, Vorapaxar, Atopaxar, F16618),[20] and peptidomimetic antagonists (RWJ-56110,[21] and RWJ-58259[22]). We first tested the effect of four PAR-1 antagonists: SCH79797, FR171113, Vorapaxar, and RWJ-56110 in response to PAR-1 agonist peptide activation in podocytes. Pre-treatment of ciPods with RWJ56110, and FR171113 prior to stimulation with PAR-1 agonist peptide significantly inhibited the signalling to JNK, VASP, ATF-2, c-Jun, SMAD2 and SMAD3. Interestingly, SCH79797 and Vorapaxar significantly inhibited JNK, ATF-2, c-Jun, SMAD2 and SMAD3, but failed to inhibit the phosphorylation of VASP (Supplementary Figure S1).

Previously, we have shown that relapse plasma of patients with FSGS induced the phosphorylation of VASP via PAR-1 receptor[9]. Here, we have extended this finding by exposure of nephrotic plasma to ciPods along with inhibiting the PAR-1 receptor by a suite of PAR-1 antagonists; RWJ56110, SCH79797, Vorapaxar, and FR171113. The phosphorylation of VASP, JNK, and proteins involved in the fibrotic pathway was then evaluated. Relapse NP-

induced JNK, VASP, ATF-2, c-Jun, SMAD2, and SMAD3 phosphorylation and this was significantly reduced when PAR-1 was inhibited by RWJ56110 and FR171113. As with PAR-1 peptide stimulation, SCH79797 and Vorapaxar failed to inhibit the activation of VASP by relapse plasma. Also, the phosphorylation of c-Jun at Ser73 induced by relapse NP was not inhibited in the presence of SCH79797. These signaling data suggest a distinct mode of agonism of PAR-1 receptor by disease plasma similar to but not completely identical to PAR-1 peptide agonism in podocytes (Figure 3).

TGF-β1 receptor inhibition efficiently inhibits SMAD-dependent signalling pathway induced by TGF-β1, but not by nephrotic plasma.

So far, we have shown that treatment of ciPods with either TGF-β1 or PAR-1 agonist or nephrotic plasma resulted in a significant increase in the phosphorylation of proteins involved in a SMAD signalling pathway, including phosphorylation of SMAD2 and SMAD3. To determine whether TGF-β1 receptor was involved in nephrotic plasma-induced activation of the signalling pathway mentioned above, SB-43152, a specific inhibitor of TGF-β1 receptor was used. SB-43152 is a selective and potent inhibitor of the TGF-β type I receptor.[23] To determine whether SB-43152 could inhibit TGF-β1 receptor in podocytes, ciPods were pre-treated for 30 minutes with 5uM and 10uM of SB-43152 and then induced with 10 ng/mL TGF-β1 for 15 minutes. High levels of phosphorylated Smad2 and Smad3 were detected in response to 15 and 30 minute-treatment with TGF-β1. These were entirely inhibited by 5uM and 10uM SB-43152 (Supplementary Figure S2). To further elucidate the role of TGF-β1 receptor in SMAD2 and SMAD3 activation by nephrotic plasma, cells were pre-incubated for 30 minutes with 5uM and 10uM SB-43152 following by 15 minutes treatment with SRNS relapse and paired-remission plasma. Compared to paired remission and untreated control, the phosphorylation of SMAD2 and SMAD3 were significantly increased in response to relapse

plasma. These effects were not blocked by the inhibition by SB-43152, suggesting that relapse plasma is not directly stimulating the TGF-β1 receptor (Figure 4). Also, the TGF-β1 receptor inhibitor failed to block the PAR-1 induced SMAD-signalling pathway (Supplementary Figure S3).

Nephrotic plasma stimulates signaling to VASP and JNK in GlomSpheres which is selectively blocked by PAR-1 antagonists

To better mimic an *in vivo* glomerulus, we utilized a novel 3D co-culture model (GlomSpheres) generated via the aggregation of conditionally immortalized human podocytes (ciPods) and glomerular endothelial cells (ciGEnCs) to form a glomerulus-like sphere. GlomSpheres associate such that the podocytes are on the outside and display a mature basement membrane with the expression of Nephrin, Podocin and COL4A3 upregulated. A branching endothelial domain is present on the inside.[15] 15% relapse and remission plasma were applied to the sequential spheroids at day 10 at different time-points, from 5 to 60 minutes. The treated GlomSpheres were then stained with phospho-VASP S157 and phospho-JNK antibodies. Increased phosphorylation of JNK and VASP were mainly seen in the podocyte compartment of GlomSpheres (Supplementary Figure S4). The fluorescence intensity of phospho-VASP and phospho-JNK was significantly increased in response to relapse plasma compared to paired-remission plasma and untreated control in a time-dependent change, reaching a maximal expression level at 15 to 45 minutes. The mean fluorescence intensity of the phosphorylation of JNK began to increase at 15 minutes and peaked at 45 minutes (Figure 5a and 5c), while the phosphorylation of VASP reached a maximum at 15 minutes (Figure 5b and 5d) after relapse plasma incubation. These responses did not occur with remission plasma treatment. These responses were significantly inhibited by the same PAR-1 antagonists as found in the 2D ciPods model (Figure 5e-5h). As seen

previously, VASP phosphorylation was not inhibited by Vorapaxar or SCH79797, unlike JNK signaling.

These data closely support the previous findings in a new disease model that more closely resembles human glomerular morphology and physiology.

Nephrotic plasma disrupts podocyte cytoskeleton and causes enhanced podocyte migration and podocyte loss

Foot process effacement and podocyte loss are major events in podocyte injury responses and the development of proteinuria. To determine if nephrotic plasma stimulates the podocytes to be more motile as a surrogate of effacement[24], a scratch assay was performed. CiPods treated with relapse plasma from seven patients had closed the scratch area significantly more compared to control or their paired remission plasma (Figure 6a and 6b). We also applied plasma from three patients to our spheroid model to explore podocyte injury in response to circulating factors in relapse plasma. Relapse and remission plasma were applied to Glomspheres at day 10 for 72 hours. The treated Glomspheres were then stained with podocin and PECAM-1 antibodies for podocyte and endothelial markers, respectively. Podocin fluorescence intensity was significantly decreased in response to relapse plasma compared to paired-remission plasma. Relapse plasma does not induce a change in PECAM-1 fluorescence, suggesting podocyte target specificity (Figure 6c and 6d). To further examine the effect of relapse plasma on podocyte injury, we then utilized Glomspheres containing GFP-tagged podocytes and ciGEnC to evaluate loss of podocytes. We found that relapse plasma significantly reduced the intensity of GFP fluorescence suggesting podocyte loss on GlomSpheres relative to paired remission and untreated control (Figure 6e and 6f). We then stained treated spheroids with phalloidin to determine intracellular actin distribution of podocyte injury induced by relapse plasma. There was a weaker fluorescence intensity and

subjectively disruption of intracellular filamentous actin after relapse plasma treatment compared to paired remission plasma and untreated control (Figure 6g and 6h).

PAR-1 inhibition inhibits nephrotic plasma-induced podocyte migration and podocyte loss

As we observed nephrotic plasma stimulation enhanced podocyte motility and podocyte loss, we next assessed if PAR-1 antagonists could prevent the nephrotic plasma-driven podocyte motility or rescue the podocyte loss. ciPods were treated with relapse plasma in the absence or presence of PAR-1 antagonists and a wound scratch assay was analyzed. As shown in Figure 7a and 7c, our data convincingly showed that PAR-1 antagonists, RWJ56110, Vorapaxar and FR17113 significantly blocked the relapse plasma-induced podocyte motility. SCH79797 did not reduce the enhanced podocyte motility in ciPods. Furthermore, we used GFP-tagged podocyte GlomSpheres treated with nephrotic plasma along with PAR-1 antagonists to quantify whether PAR-1 antagonists could rescue the podocyte loss in GlomSpheres. Consistently, relapse plasma-induced podocyte loss was significantly inhibited in the presence of PAR-1 antagonists, RWJ56110, Vorapaxar and FR17113, but not SCH79797 (Figure 7b and 7d).

Nephrotic plasma stimulates signaling to VASP and proteins involved in fibrotic processes in kidney organoids

A more complex and representative model of the human kidney is the pluripotent stem cell derived kidney organoid, which contains patterning and segmenting nephrons surrounded by a renal stroma[17]. We have previously described the accuracy of human kidney organoid glomeruli at the level of cellular complexity and protein and transcriptional congruence,[25] and have used organoids and organoid glomeruli to model glomerular disease.[25,26] Here, we generated kidney organoids from human iPSCs, treated whole organoids with 15% nephrotic plasma at Day 25 for 15 minutes and evaluated the

phosphorylation of VASP and JNK. Differences in staining for phospho-JNK and phospho-VASP were observed within the glomeruli of organoids treated with relapse plasma, paired-remission plasma, and untreated. Relapse plasma increased the phosphorylation of JNK (Figure 8a and 8b) and VASP (Figure 8c and 8d) compared with paired-remission plasma and untreated. The co-localization of pVASP and nephrin and pJNK and nephrin was observed within the podocytes of relapse plasma-treated organoids (Supplementary Video S1). This co-localization did not occur in the podocytes from untreated or remission plasma-treated organoids. The increased phosphorylation of VASP and JNK in organoids treated with relapse plasma was confirmed by Western blot analysis of whole organoids. Furthermore, the activation of the signaling to ATF-2, c-Jun, SMAD2, and SMAD3 in response to relapse plasma was detected in kidney organoids, as had been identified in ciPods (Figure 8e).

Nephrotic plasma induces loss of podocyte markers in kidney organoids

There is evidence to suggest that kidney organoids can be used for renal disease modelling or nephrotoxic drug screening.[25] We, therefore, utilized the kidney organoids to investigate the effect of nephrotic plasma on podocyte injury in kidney organoids, and observe if podocyte loss or dedifferentiation is seen alongside the described pro-fibrotic signalling changes. The organoids were treated with relapse and paired-remission plasma for 24 hours, and podocyte-specific markers were examined. The organoids treated with relapse plasma significantly reduced the expression of podocyte markers including nephrin, podocin, and WT1 (Figure 9). This could be due to either fewer glomeruli or less expression of these markers in individual glomeruli.

A summary of the key findings is presented in Table 1.

Table 1: A summary table of the results in this study

Experimental Conditions	Results	Cell-based models		
		ciPods	GlomSpheres	Kidney Organoids
	Signaling Pathways			
PAR-1 agonist	VASP	↑	N/A	N/A
	JNK	↑	N/A	N/A
	ATF-2	↑	N/A	N/A
	c-jun	↑	N/A	N/A
	SMAD-2	↑	N/A	N/A
	SMAD-3	↑	N/A	N/A
Relapse plasma	VASP	↑	↑	↑
	JNK	↑	↑	↑
	ATF-2	↑	N/A	↑
	c-jun	↑	N/A	↑
	SMAD-2	↑	N/A	↑
	SMAD-3	↑	N/A	↑
PAR-1 agonist + SCH79797	VASP	↔	N/A	N/A
	JNK	↓	N/A	N/A
	ATF-2	↓	N/A	N/A
	c-jun	↓	N/A	N/A
	SMAD-2	↓	N/A	N/A
	SMAD-3	↓	N/A	N/A
PAR-1 agonist + FR171113	VASP	↓	N/A	N/A
	JNK	↓	N/A	N/A
	ATF-2	↓	N/A	N/A
	c-jun	↓	N/A	N/A
	SMAD-2	↓	N/A	N/A
	SMAD-3	↓	N/A	N/A
PAR-1 agonist + Vorapaxar	VASP	↔	N/A	N/A
	JNK	↓	N/A	N/A
	ATF-2	↓	N/A	N/A
	c-jun	↓	N/A	N/A
	SMAD-2	↓	N/A	N/A
	SMAD-3	↓	N/A	N/A
PAR-1 agonist + RWJ-56110	VASP	↓	N/A	N/A
	JNK	↓	N/A	N/A
	ATF-2	↓	N/A	N/A
	c-jun	↓	N/A	N/A
	SMAD-2	↓	N/A	N/A
	SMAD-3	↓	N/A	N/A
Relapse plasma + SCH79797	VASP	↔	↔	N/A
	JNK	↓	↓	N/A
	ATF-2	↓	N/A	N/A
	c-jun	↔	N/A	N/A
	SMAD-2	↓	N/A	N/A
	SMAD-3	↓	N/A	N/A

Relapse plasma + FR171113	VASP	↓	↓	N/A
	JNK	↓	↓	N/A
	ATF-2	↓	N/A	N/A
	c-jun	↓	N/A	N/A
	SMAD-2	↓	N/A	N/A
	SMAD-3	↓	N/A	N/A
Relapse plasma + Vorapaxar	VASP	↔	↓	N/A
	JNK	↓	↓	N/A
	ATF-2	↓	N/A	N/A
	c-jun	↓	N/A	N/A
	SMAD-2	↓	N/A	N/A
	SMAD-3	↓	N/A	N/A
Relapse plasma + RWJ-56110	VASP	↓	↓	N/A
	JNK	↓	↓	N/A
	ATF-2	↓	N/A	N/A
	c-jun	↓	N/A	N/A
	SMAD-2	↓	N/A	N/A
	SMAD-3	↓	N/A	N/A
TGF-β1	SMAD-2	↑	N/A	N/A
	SMAD-3	↑	N/A	N/A
TGF-β1 + SB-43152	SMAD-2	↑	N/A	N/A
	SMAD-3	↑	N/A	N/A
PAR-1 agonist + SB-43152	SMAD-2	↓	N/A	N/A
	SMAD-3	↓	N/A	N/A
	Podocyte motility			
Relapse plasma		↑	↑	N/A
Relapse plasma + SCH79797		↔	↔	N/A
Relapse plasma + FR171113		↓	↓	N/A
Relapse plasma + Vorapaxar		↓	↓	N/A
Relapse plasma + RWJ-56110		↓	↓	N/A
	Podocyte Loss			
Relapse plasma		N/A	↑	↑
Relapse plasma + SCH79797		N/A	↔	N/A
Relapse plasma + FR171113		N/A	↓	N/A
Relapse plasma + Vorapaxar		N/A	↓	N/A
Relapse plasma + RWJ-56110		N/A	↓	N/A

↑ = increase, ↓ = decrease, ↔ = no change

Discussion

It is known that a circulating factor targets podocytes leading to podocyte injury and proteinuria.[6] However, the mechanism whereby a circulating factor affects podocytes has not been thoroughly explored. This study was designed to further elucidate the signalling pathways mediated by a circulating factor in podocytes by exposure of ciPods and GlomSpheres to nephrotic plasma and the contribution of PAR-1 to nephrotic plasma-induced podocyte injury. We demonstrate that pro-fibrotic signalling is induced downstream of the PAR-1 signalling cascade, which corresponds with functional effects of podocyte motility, detachment, and loss of differentiation.

There is evidence suggesting that TGF-β1 plays a significant role as a pro-fibrotic mediator and is associated with PAR regulation in fibrotic diseases.[27] Activation of PAR-1 has been reported to play a major role in inducing pro-inflammatory and pro-fibrotic effects in bleomycin-induced lung injury.[28] We, therefore, assessed the effects of nephrotic plasma in the activation of fibrotic mechanisms in podocytes. In the current study, we firstly demonstrated that plasma from 11 patients with post-transplant recurrence of SRNS induces VASP, JNK, and SMAD signalling in podocytes (Figure 1). Activation of the signalling pathways induced by TGF-β and PAR-1 and PAR-2 agonists have been associated with tissue fibrosis and cancer. This crosstalk interacts via several mechanisms, including mutual regulation of ligand–ligand, ligand-receptor, and receptor–receptor at the transcriptional, post-transcriptional, and receptor transactivation levels.[19] However, a direct interaction between PAR-1 and TGF-β1 in kidney disease has not been fully understood. We examined if PAR-1 agonist peptide and TGF-β1 initiate the same response as the nephrotic plasma in podocytes. We found that treatment of ciPods with PAR-1 agonist peptide and TGF-β1 resulted in rapid phosphorylation of VASP, JNK, ATF-2, c-Jun, SMAD2, and SMAD3 compared to untreated control which is

consistent with the response of SRNS relapse plasma (Figure 2). It is interesting to note that PAR-1 agonist peptide induced the phosphorylation of c-Jun, SMAD2, and SMAD3 earlier than TGF-β1, suggesting the activation occurs through different pathways, and TGF-β1 receptor inhibition did not inhibit PAR-1 peptide stimulation (Supplementary Figure S3). Together, these results suggest activation of pathways downstream of TGF-β1 that are initiated at the PAR-1 receptor. We also determined the effect of nephrotic plasma on a new glomerular spheroid model (GlomSpheres) and kidney organoids which demonstrate much improved molecular and morphological features of an *in vivo* glomerulus. Applying relapse plasma to GlomSpheres significantly induced the signalling to VASP and JNK in a time-dependent manner (Figure 5). Interestingly, the stimulation of signaling to VASP, JNK, and proteins in the fibrosis pathway was also detected in kidney organoids (Figure 8). These data are completely consistent with the finding on a ciPods 2D model.

Prior studies have noted the role of PAR-1 receptor in response to relapse plasma.[9] PAR-1 receptors adopt a spectrum of distinct structural conformations upon receptor proteolysis that defines the extent and direction of their signaling activity. PAR signaling outputs are generated by receptor proteolysis at different receptor sites by distinct proteases, in turn allowing individual PARs to mediate pleiotropic cellular signaling events.[29] Canonical signalling is defined by thrombin-mediated PAR1 activation, which involves the generation of a tethered ligand upon cleavage of the peptide bond between Arg-41 and Ser-42. Here, we selected four PAR-1 antagonists, RWJ56110, SCH79797, Vorapaxar, and FR171113 to inhibit the PAR-1 receptor before treatment with PAR-1 agonist peptide. RWJ56110 is a potent peptide-mimetic antagonist which directly inhibits PAR-1 activation and internalization by interrupting the binding of the tethered ligand to PAR-1 receptor.[21,30] Similarly, SCH79797, Vorapaxar, and FR171113 are identified as small molecules which act as competitive

inhibitors targeting the tethered ligand site and competing with serine proteases.[20] The exact site of action of these inhibitors is not known, so limiting our ability to fine map PAR-1 activation using these tools. We found that, following stimulation of PAR-1 by PAR-1 antagonists, RWJ56110 and FR171113 significantly reduced the signalling to JNK, VASP, ATF-2, c-Jun, SMAD2 and SMAD3. Surprisingly, SCH79797 and Vorapaxar significantly inhibited JNK, ATF-2, c-Jun, SMAD2 and SMAD3, but failed to inhibit the phosphorylation of VASP (Supplementary Figure S1). A recent phosphoproteomic study shows that VASP is activated by thrombin in endothelial cells, but not by activated protein C (APC).[31] The latter cleaves PAR-1 at a distinct extracellular site, resulting in non-canonical signalling pathways. Therefore, VASP phosphorylation is likely a consequence of PAR-1 canonical signalling pathways.

Next, we examined the role of PAR-1 in the mechanism of action of relapse plasma in podocytes. We first show that RWJ56110 and FR171113 significantly block relapse plasma-induced JNK, VASP, ATF-2, c-Jun, SMAD2, and SMAD3 phosphorylation. As before, SCH79797 and Vorapaxar did not reduce the signaling to VASP by relapse plasma. Additionally, this time the signaling to c-Jun by relapse plasma was not inhibited by SCH79797 (Figure 3). The effects of PAR-1 inhibition on phosphorylation of VASP and JNK in response to relapse plasma in GlomSpheres were explored. The observed effects of PAR-1 antagonists in GlomSpheres are comparable to those noticed in the ciPod model, with selective inhibition of VASP as before (Figure 5). Overall, these inhibitor data suggest a consistent and discrete consequence of PAR-1 receptor activation by disease plasma in its signaling to VASP. Although all four PAR-1 antagonists used in our study are ligand-binding site competitors, we find they differentially antagonize downstream signaling pathways with VASP phosphorylation not inhibited by either vorapaxar or SCH79797. The reasons for this difference are currently unclear but may

be due to the mode of antagonist-receptor binding. A vorapaxar-inhibited conformation of PAR1 is the only structure solved by X-ray crystallography[32] with more recent dynamic single-molecule force spectroscopy further revealing how this drug stabilizes the inactive state of the receptor[33]. Whether RWJ56110 and FR171113 binding induce a different receptor conformation that allows them to more effectively antagonize all downstream PAR-1 receptor signaling, including VASP phosphorylation, is well beyond the scope of this current paper.

There is a report that TGF- β1 is elevated in children with SRNS compared with healthy controls.[34] Thus a high level of TGF- β1 could be involved in the pathogenesis of idiopathic nephrotic syndrome and could be associated with failed response to corticosteroids. We hypothesized that the circulating factor in relapse plasma of SRNS patients is not TGF- β1. Hence, we examined this assumption by inhibiting the TGF- β1 receptor by SB-43152, an effective specific inhibitor. SB-43152 completely inhibited SMAD2 and SMAD3 signalling induced by TGF- β1 in podocytes (Supplemental Figure 2). Importantly, we found that there was no statistically significant difference in SMAD2 and SMAD3 phosphorylation induced by nephrotic plasma (Figure 4). We, therefore, assumed that the unknown circulating factor in SRNS relapse plasma is not TGF- β1.

Mechanistically, we show an increase in podocyte motility in ciPods in response to relapse plasma (Figure 6) supporting our previous study that a circulating factor has a direct effect on podocyte migration via the phosphorylation of VASP.[9] PAR-1 inhibitors; RWJ56110, Vorapaxar, and FR17113 effectively reduced the enhanced podocyte migration-induced by relapse plasma but not SCH79797, confirming the differential signalling discussed above has functional consequences. (Figure 7).

We also evaluated the effects of nephrotic plasma on podocyte loss in GlomSpheres and kidney organoids. We show the first time here that relapse plasma significantly enhanced

podocyte loss in GlomSpheres (Figure 6) and loss of podocyte markers suggestive of podocyte loss or dedifferentiation in kidney organoids (Figure 9), and the derangement of actin (Figure 6). Relapse plasma induced-podocyte loss was rescued by PAR-1 antagonists suggesting the involvement of PAR-1 in mediating podocyte injury (Figure 7). The present findings are consistent with previous reports that demonstrated the contribution of PAR-1 to development of podocyte and glomerular injury and diabetic nephropathy.[35–37]

Taken together, our data suggest that the circulating factor in relapse plasma from patients with SRNS can activate PAR-1, leading to the phosphorylation of VASP, JNK, and proteins associated with fibrotic responses in podocytes. Activation of JNK by circulating factor might phosphorylate SMAD2 and SMAD3 via the phosphorylation of ATF-2 and c-Jun or directly activate SMAD2 and SMAD3, leading to kidney fibrosis or podocyte injury. We propose that these signalling responses may lead to enhanced podocyte motility, and podocyte loss leading to podocyte injury (Figure 10). Importantly, they suggest a potential use of antifibrotic agents, that can be tested utilizing the enhanced models we have established and demonstrated here. However, the precise mechanism of these findings needs to be further developed.

METHODS

Cell culture

Conditionally immortalized wild-type human podocyte (ciPods) and conditionally immortalized human glomerular endothelial cells (ciGEnCs) developed by Saleem *et al*.,[38] and Satchell *et al*.,[39] respectively were used in this study. ciPods were cultured in RPMI 1640 supplemented with 10% foetal bovine serum and 1% penicillin/streptomycin. ciGEnCs were cultured in EBM-2 media (Lonza, CC-3156) supplemented with EGM-2 Endothelial Cell Growth Medium-2 BulletKit). Both cells were cultured at the permissive temperature (33°C) for 3-4

days or until 70-80% confluency and subsequently moved to non-permissive temperature (37°C) for 10-14 days to allow differentiation before being used experimentally. All cells were tested negative for mycoplasma infection.

Podocyte cell treatments

Nephrotic plasma samples (Supplementary Table S1) were processed and carried out as previously described.[9] ciPods were treated with 15% nephrotic plasma for 15 minutes, 15 uM of PAR-1 selective agonist peptide (Thr-Phe-Leu-Leu-Arg-NH2 (TFLLR-NH2)) and 10 ng/mL of TGF-β1 at different time points at 37°C. To inhibit PAR-1 receptor, ciPods were pre-treated with four PAR-1 antagonists, 10 uM RWJ56110, 150 nM SCH79797, 100 nM Vorapaxar, and 15 uM FR171113 for 30 minutes and subsequently stimulated by PAR-1 agonist peptide (PAR-1 AP) or nephrotic plasma for 15 minutes. For inhibition of TGF-β1 receptor, the cells were pre-treated with 5 and 10 nM of SB431542, a specific inhibitor of TGF-βRI for 30 minutes before induction with 10 ng/mL of TGF-β1 or nephrotic plasma for 15 minutes. Additional details of treatment are provided in the Supplementary Materials and Methods.

Generation of GlomSpheres and treatments

Our group has developed a 3D glomerulus-like structure spheroid model (GlomSpheres) which is a co-culture of human ciPods and ciGEnCs using magnetic nanoparticles to induce self-organization.[15] Detailed protocols are described in the Supplementary Materials and Methods. GlomSpheres were treated with 15% of nephrotic plasma at different time points (5, 15, 30, 45, and 60 minutes) at 37°C to investigate whether the circulating factor could stimulate the same signalling pathways as in ciPods. Additionally, the 3D co-culture of GFP-tagged podocytes[7] and ciGEnCs spheroids was used for the investigation of the effect of circulating factor on podocyte loss. The GFP-tagged spheroids were treated with 15% of

nephrotic plasma for 7 days at 37°C and imaged on the Leica DM IRB microscope and images captured using Zeiss Axiocam ERc 5S camera for fluorescence intensity analysis.

Immunofluorescence staining of GlomSpheres

Immunofluorescence techniques are provided in the Supplementary Materials and Methods.

Generation and treatment of human induced pluripotent stem cell (iPSC)-derived kidney organoids

Kidney organoids were differentiated from a human episomally-reporgrammed iPSC Line (A18945, ThermoFisher Scientific) using a previously described stepwise differentiation protocol from the works of Takasako *et al*.[16] and Howden and Little[40] with slight modifications. Detailed protocols are described in the Supplementary Materials and Methods.

Whole-mount kidney organoids immunofluorescence

Immunofluorescence techniques for whole-mount kidney organoids are provided in the Supplementary Materials and Methods.

Western blot analysis

Western blotting was carried out following standard protocols. Additional details are provided in the Supplementary Materials and Methods.

Scratch assay

A scratch injury was performed using a sterile 200uL pipette tip and images of the scratch were taken after 15 hours, as previously described.[9]

Statistical analysis

Each experiment was carried out in triplicate. Graphs illustrating mean and standard deviation (mean ± SD) dot plots were generated by GraphPad Prism 8.4.2 (GraphPad Software, Inc, CA, USA). The one-way ANOVA followed by Tukey's Multiple Comparison Test was used to

evaluate the statistical significance where there were more than two groups to compare. T-test was used to determine the significance between the means of two groups. A P-value < 0.05 was indicated to be significant.

AUTHOR CONTRIBUTIONS

M.A.S and G.I.W designed the study and reviewed the manuscript; M.C carried out experiments, made the figures, analyzed data, drafted and revised the paper; J.T, and C.J.M assisted with image acquisition and data analyses; M.H.L and I.G. assisted with kidney organoid studies and M.H.L. reviewed the manuscript.

ACKNOWLEDGEMENTS

This study was supported by the Royal Thai Government Scholarship program, the Nephrotic Syndrome Trust (www.nstrust.co.uk) and Medical Research Council awards, MR/R013942/1, and MR/R003017/1. MHL holds an NHMRC Senior Principal Research Fellowship from the National Health and Medical Research Council of Australia (GNT1136085). We thank the clinicians who facilitated the sample collection, the patients and their families for participating in this study, and to Dr. Maryam Afzal and Tim Roberts for organizing the sample in Bristol Renal unit. We thank Professor Stuart Mundell (University of Bristol) for valuable discussions on PAR-1 signalling. We also thank the Wolfson Bioimaging Facility for their support and assistance in this work.

DISCLOSURES

None

SUPPLEMENTAL MATERIALS

Supplementary Table S1: Patient clinical details

Supplementary Figure S1: Effect of PAR-1 antagonists on JNK, VASP, ATF-2, c-Jun, SMAD3, and SMAD2 phosphorylation activation by PAR-1 agonist peptide

Supplementary Figure S2: SB-431542 efficiently inhibits SMAD phosphorylation induced by TGF-β1 in podocytes.

Supplementary Figure S3: TGF-β1 receptor inhibitor does not inhibit SMAD phosphorylation induced by PAR-1 agonist peptide in podocytes.

Supplementary Figure S4: Phospho-VASP and phosphor-JNK mainly expresses in podocyte compartment of GlomSpheres

REFERENCES:

1. Noone DG, Iijima K, Parekh R. Idiopathic nephrotic syndrome in children. *The Lancet*. 2018;392(10141):61-74.

2. Saleem MA. Molecular stratification of idiopathic nephrotic syndrome. *Nat Rev Nephrol*. 2019;15(12):750-765.

3. Nourbakhsh N, Mak RH. Steroid-resistant nephrotic syndrome: past and current perspectives. *Pediatr Health Med Ther*. 2017;8:29-37.

4. Lee JM, Kronbichler A, Shin JI, Oh J. Current understandings in treating children with steroid-resistant nephrotic syndrome. *Pediatr Nephrol*. Published online February 21, 2020.

5. Morello W, Puvinathan S, Puccio G, et al. Post-transplant recurrence of steroid resistant nephrotic syndrome in children: the Italian experience. *J Nephrol*. Published online October 15, 2019.

6. Ding WY, Saleem MA. Current concepts of the podocyte in nephrotic syndrome. *Kidney Res Clin Pract*. 2012;31(2):87-93.

7. Lennon R, Singh A, Welsh GI, et al. Hemopexin Induces Nephrin-Dependent Reorganization of the Actin Cytoskeleton in Podocytes. *J Am Soc Nephrol JASN*. 2008;19(11):2140-2149.

8. Wei C, El Hindi S, Li J, et al. Circulating urokinase receptor as a cause of focal segmental glomerulosclerosis. *Nat Med*. 2011;17(8):952-960.

9. Harris JJ, McCarthy HJ, Ni L, et al. Active proteases in nephrotic plasma lead to a podocin-dependent phosphorylation of VASP in podocytes via protease activated receptor-1. *J Pathol*. 2013;229(5):660-671.

10. Heuberger DM, Schuepbach RA. Protease-activated receptors (PARs): mechanisms of action and potential therapeutic modulators in PAR-driven inflammatory diseases. *Thromb J*. 2019;17(1):4.

11. Hollenberg MD, Mihara K, Polley D, et al. Biased signalling and proteinase-activated receptors (PARs): targeting inflammatory disease. *Br J Pharmacol*. 2014;171(5):1180-1194.

12. Zhao P, Metcalf M, Bunnett NW: Biased Signaling of Protease-Activated Receptors. *Front. Endocrinol.* 5: 67, 2014

13. van den Eshof BL, Hoogendijk AJ, Simpson PJ, et al. Paradigm of Biased PAR1 (Protease-Activated Receptor-1) Activation and Inhibition in Endothelial Cells Dissected by Phosphoproteomics. *Arterioscler Thromb Vasc Biol*. 2017;37(10):1891-1902.

14. May CJ, Welsh GI, Chesor M, et al. Human Th17 cells produce a soluble mediator that increases podocyte motility via signaling pathways that mimic PAR-1 activation. *Am J Physiol-Ren Physiol*. 2019;317(4):F913-F921.

15. Tuffin J, Chesor M, Kuzmuk V, et al. GlomSpheres as a 3D co-culture spheroid model of the kidney glomerulus for rapid drug-screening. *Commun Biol*. 2021;4(1):1-14.

16. Takasato M, Er PX, Chiu HS, Little MH. Generation of kidney organoids from human pluripotent stem cells. *Nat Protoc*. 2016;11(9):1681-1692.

17. Grynberg K, Ma FY, Nikolic-Paterson DJ: The JNK Signaling Pathway in Renal Fibrosis. *Front. Physiol.* 8: 829, 2017

18. Biernacka A, Dobaczewski M, Frangogiannis NG. TGF-β signaling in fibrosis. *Growth Factors Chur Switz*. 2011;29(5):196-202.

19. Ungefroren H, Gieseler F, Kaufmann R, Settmacher U, Lehnert H, Rauch BH. Signaling Crosstalk of TGF-β/ALK5 and PAR2/PAR1: A Complex Regulatory Network Controlling Fibrosis and Cancer. *Int J Mol Sci*. 2018;19(6):1568.

20. Flaumenhaft R, De Ceunynck K. Targeting PAR1: Now what? *Trends Pharmacol Sci*. 2017;38(8):701-716.

21. Andrade-Gordon P, Maryanoff BE, Derian CK, et al. Design, synthesis, and biological characterization of a peptide-mimetic antagonist for a tethered-ligand receptor. *Proc Natl Acad Sci*. 1999;96(22):12257-12262.

22. Robinson E, Knight E, Smoktunowicz N, et al. Identification of an active metabolite of PAR-1 antagonist RWJ-58259 and synthesis of analogues to enhance its metabolic stability. *Org Biomol Chem*. 2016;14(12):3198-3201.

23. Inman GJ, Nicolás FJ, Callahan JF, et al. SB-431542 Is a Potent and Specific Inhibitor of Transforming Growth Factor-β Superfamily Type I Activin Receptor-Like Kinase (ALK) Receptors ALK4, ALK5, and ALK7. *Mol Pharmacol*. 2002;62(1):65-74.

24. Welsh GI, Saleem MA. The podocyte cytoskeleton--key to a functioning glomerulus in health and disease. *Nat Rev Nephrol*. 2011;8(1):14-21.

25. Hale LJ, Howden SE, Phipson B, et al. 3D organoid-derived human glomeruli for personalised podocyte disease modelling and drug screening. *Nat Commun*. 2018;9(1):5167.

26. Majmundar AJ, Buerger F, Forbes TA, et al. Recessive NOS1AP variants impair actin remodeling and cause glomerulopathy in humans and mice. *Sci Adv*. 2021;7(1):eabe1386.

27. Lin C, von der Thüsen J, Daalhuisen J, et al. Protease-activated receptor (PAR)-2 is required for PAR-1 signalling in pulmonary fibrosis. *J Cell Mol Med*. 2015;19(6):1346-1356.

28. Howell DCJ, Johns RH, Lasky JA, et al. Absence of Proteinase-Activated Receptor-1 Signaling Affords Protection from Bleomycin-Induced Lung Inflammation and Fibrosis. *Am J Pathol*. 2005;166(5):1353-1365.

29. Fox OW, Preston RJS. Molecular basis of protease-activated receptor 1 signaling diversity. *J Thromb Haemost*. 2020;18(1):6-16.

30. Maryanoff BE, Zhang HC, Andrade-Gordon P, Derian CK. Discovery of potent peptide-mimetic antagonists for the human thrombin receptor, protease-activated receptor-1 (PAR-1). *Curr Med Chem Cardiovasc Hematol Agents*. 2003;1(1):13-36.

31. Lin Y, Wozniak JM, Grimsey NJ, et al. Phosphoproteomic analysis of protease-activated receptor-1 biased signaling reveals unique modulators of endothelial barrier function. *Proc Natl Acad Sci*. 2020;117(9):5039-5048.

32. Zhang C, Srinivasan Y, Arlow DH, et al. High-resolution crystal structure of human Protease-Activated Receptor 1 bound to the antagonist vorapaxar. *Nature*. 2012;492(7429):387-392.

33. Spoerri PM, Kato HE, Pfreundschuh M, et al. Structural Properties of the Human Protease-Activated Receptor 1 Changing by a Strong Antagonist. *Struct Lond Engl 1993*. 2018;26(6):829-838.e4.

34. Souto MFO, Teixeira AL, Russo RC, et al. Immune Mediators in Idiopathic Nephrotic Syndrome: Evidence for a Relation Between Interleukin 8 and Proteinuria. *Pediatr Res*. 2008;64(6):637-642.

35. Guan Y, Nakano D, Zhang Y, et al. A protease-activated receptor-1 antagonist protects against podocyte injury in a mouse model of nephropathy. *J Pharmacol Sci*. 2017;135(2):81-88.

36. Waasdorp M, Duitman J, Florquin S, Spek CA. Protease-activated receptor-1 deficiency protects against streptozotocin-induced diabetic nephropathy in mice. *Sci Rep*. 2016;6(1):33030.

37. Madhusudhan T, Ghosh S, Wang H, et al. Podocyte Integrin-β3 and Activated Protein C Coordinately Restrict RhoA Signaling and Ameliorate Diabetic Nephropathy. *J Am Soc Nephrol*. 2020;31(8):1762-1780.

38. Saleem MA, O'Hare MJ, Reiser J, et al. A Conditionally Immortalized Human Podocyte Cell Line Demonstrating Nephrin and Podocin Expression. *J Am Soc Nephrol*. 2002;13(3):630-638.

39. Satchell SC, Tasman CH, Singh A, et al. Conditionally immortalized human glomerular endothelial cells expressing fenestrations in response to VEGF. *Kidney Int*. 2006;69(9):1633-1640.

40. Howden SE, Little MH. Generating Kidney Organoids from Human Pluripotent Stem Cells Using Defined Conditions. *Methods Mol Biol Clifton NJ*. 2020;2155:183-192.

FIGURES

Figure 1

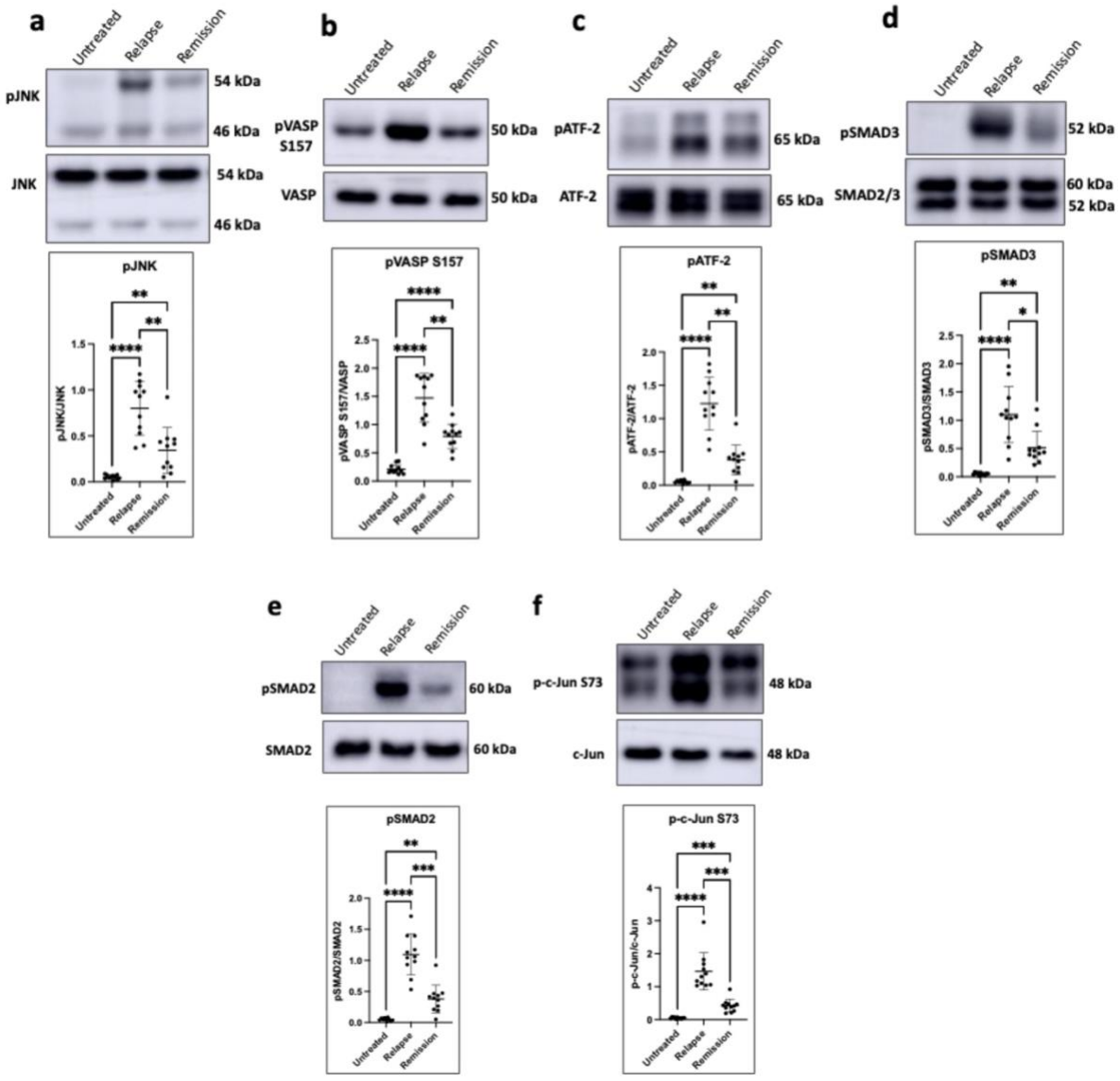

Figure 2

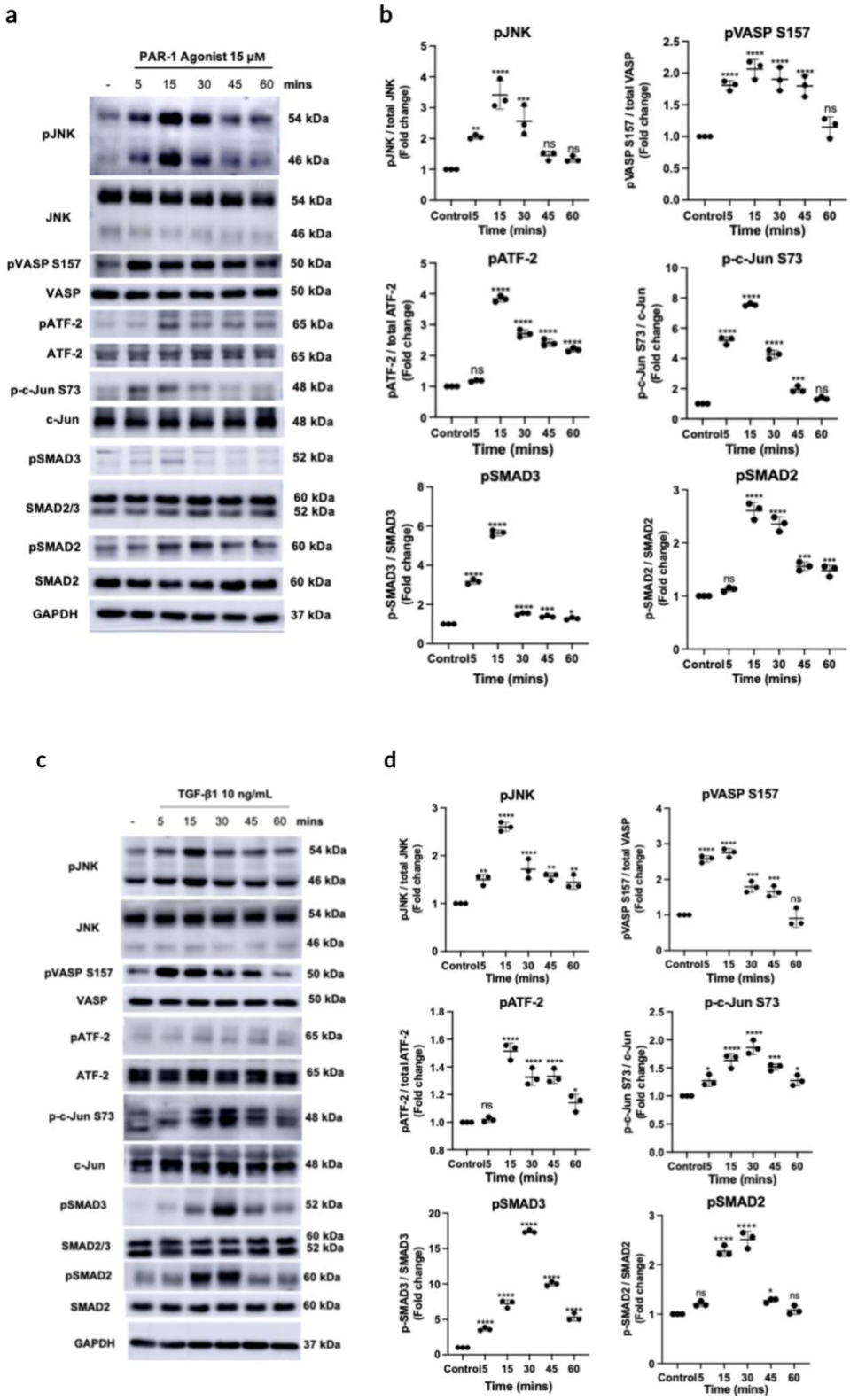
a
PAR-1 Agonist 15 μM
- 5 15 30 45 60 mins
pJNK
54 kDa
46 kDa
JNK
54 kDa
46 kDa
pVASP S157
50 kDa
VASP
50 kDa
pATF-2
65 kDa
ATF-2
65 kDa
p-c-Jun S73
48 kDa
c-Jun
48 kDa
pSMAD3
52 kDa
SMAD2/3
60 kDa
52 kDa
pSMAD2
60 kDa
SMAD2
60 kDa
GAPDH
37 kDa
b
pJNK
pJNK / total JNK (Fold change)
pVASP S157
pVASP S157 / total VASP (Fold change)
pATF-2
pATF-2 / total ATF-2 (Fold change)
p-c-Jun S73
p-c-Jun S73 / c-Jun (Fold change)
pSMAD3
p-SMAD3 / SMAD3 (Fold change)
pSMAD2
p-SMAD2 / SMAD2 (Fold change)
Control 5 15 30 45 60
Time (mins)
c
TGF-β1 10 ng/mL
- 5 15 30 45 60 mins
pJNK
54 kDa
46 kDa
JNK
54 kDa
46 kDa
pVASP S157
50 kDa
VASP
50 kDa
pATF-2
65 kDa
ATF-2
65 kDa
p-c-Jun S73
48 kDa
c-Jun
48 kDa
pSMAD3
52 kDa
SMAD2/3
60 kDa
52 kDa
pSMAD2
60 kDa
SMAD2
60 kDa
GAPDH
37 kDa
d
pJNK
pJNK / total JNK (Fold change)
pVASP S157
pVASP S157 / total VASP (Fold change)
pATF-2
pATF-2 / total ATF-2 (Fold change)
p-c-Jun S73
p-c-Jun S73 / c-Jun (Fold change)
pSMAD3
p-SMAD3 / SMAD3 (Fold change)
pSMAD2
p-SMAD2 / SMAD2 (Fold change)
Control 5 15 30 45 60
Time (mins)

Figure 3

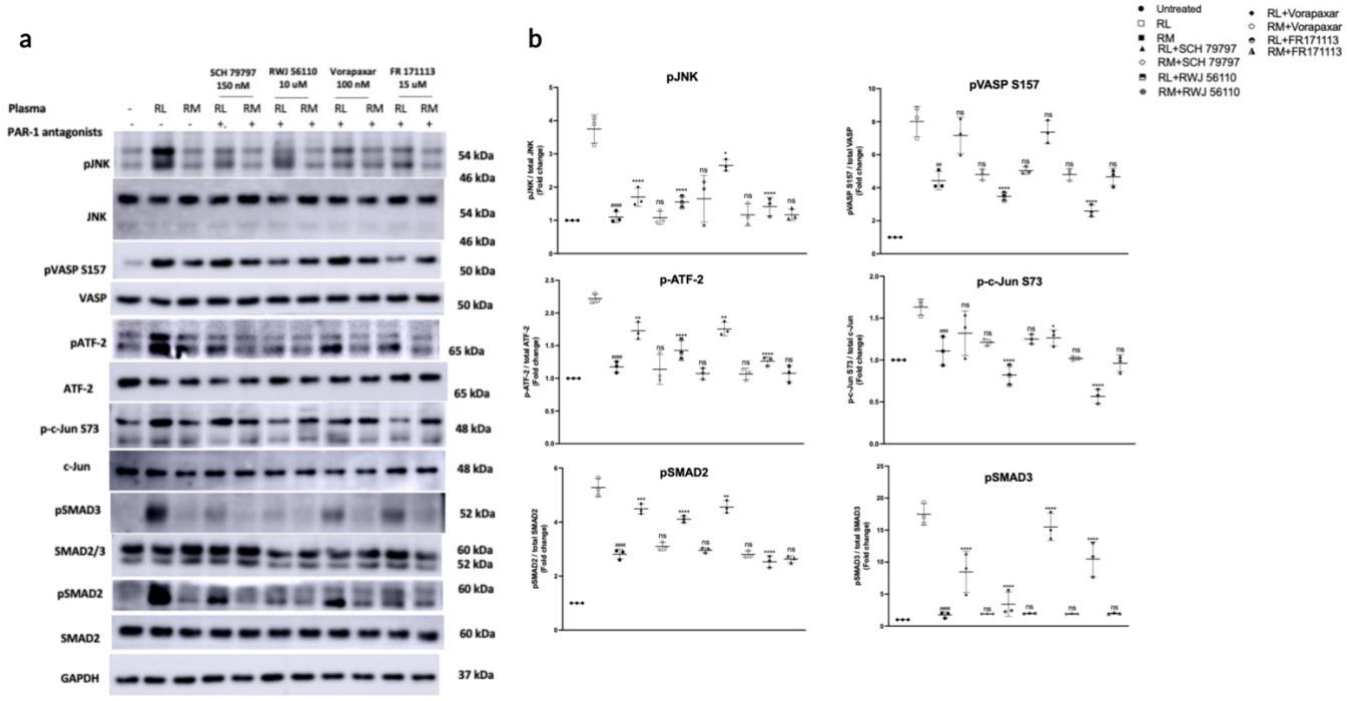

Figure 4

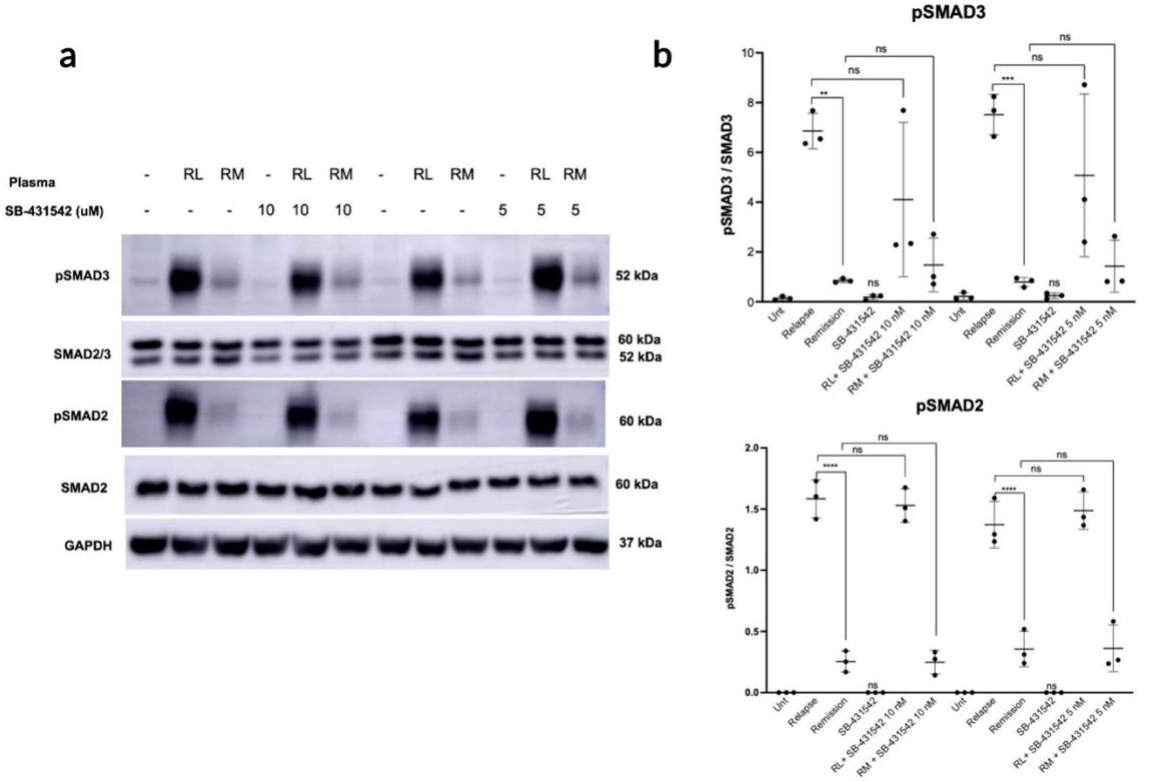

Figure 5

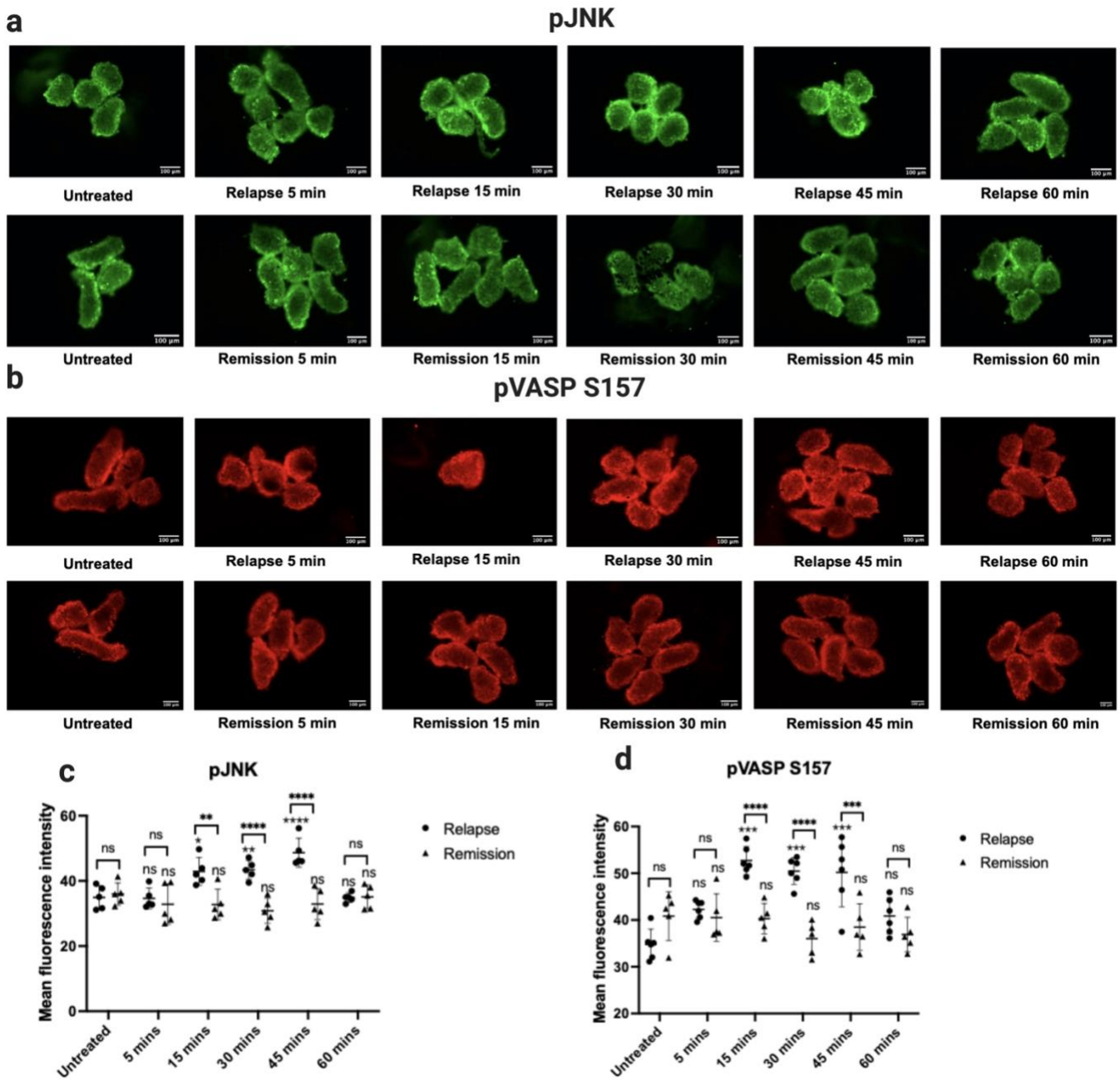
a
pJNK
Untreated
Relapse 5 min
Relapse 15 min
Relapse 30 min
Relapse 45 min
Relapse 60 min
Untreated
Remission 5 min
Remission 15 min
Remission 30 min
Remission 45 min
Remission 60 min
b
pVASP S157
Untreated
Relapse 5 min
Relapse 15 min
Relapse 30 min
Relapse 45 min
Relapse 60 min
Untreated
Remission 5 min
Remission 15 min
Remission 30 min
Remission 45 min
Remission 60 min
c
pJNK
Mean fluorescence intensity
Relapse
Remission
Untreated
5 mins
15 mins
30 mins
45 mins
60 mins
d
pVASP S157
Mean fluorescence intensity
Relapse
Remission
Untreated
5 mins
15 mins
30 mins
45 mins
60 mins

Figure 5 cont.

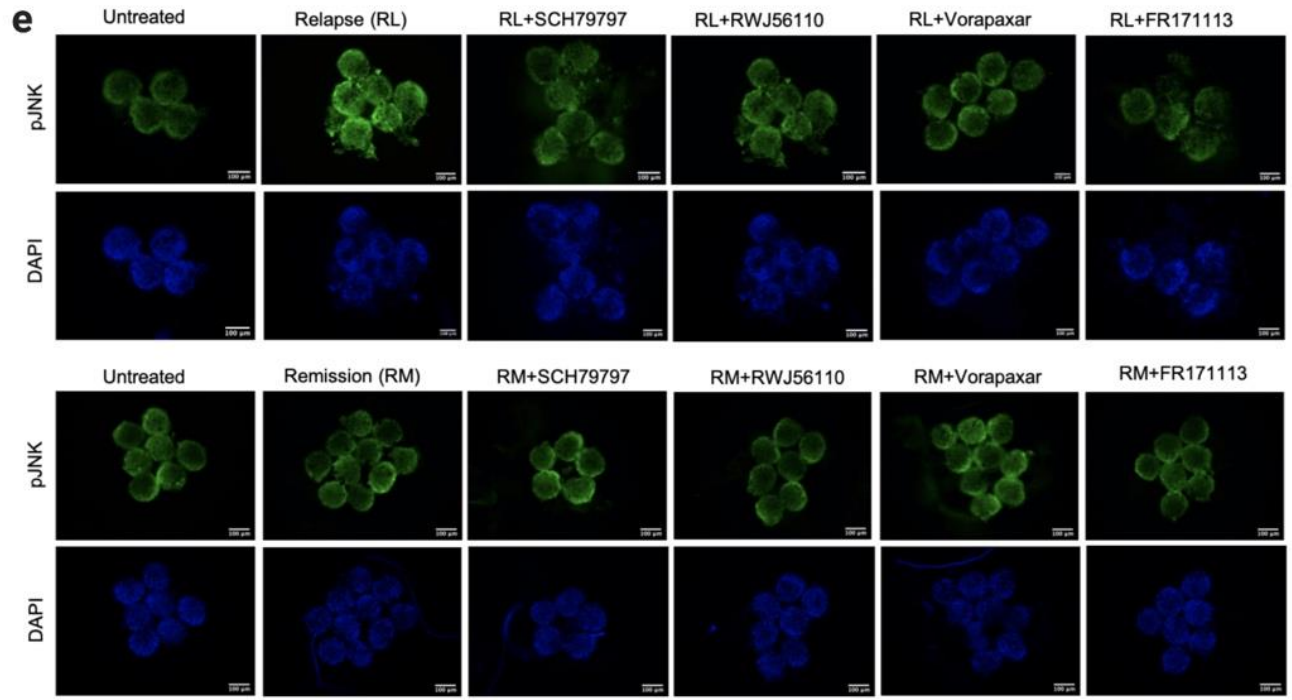

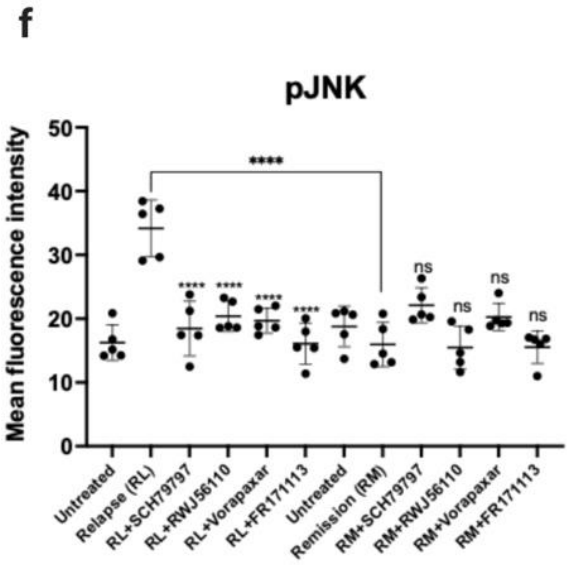

Figure 5 cont.

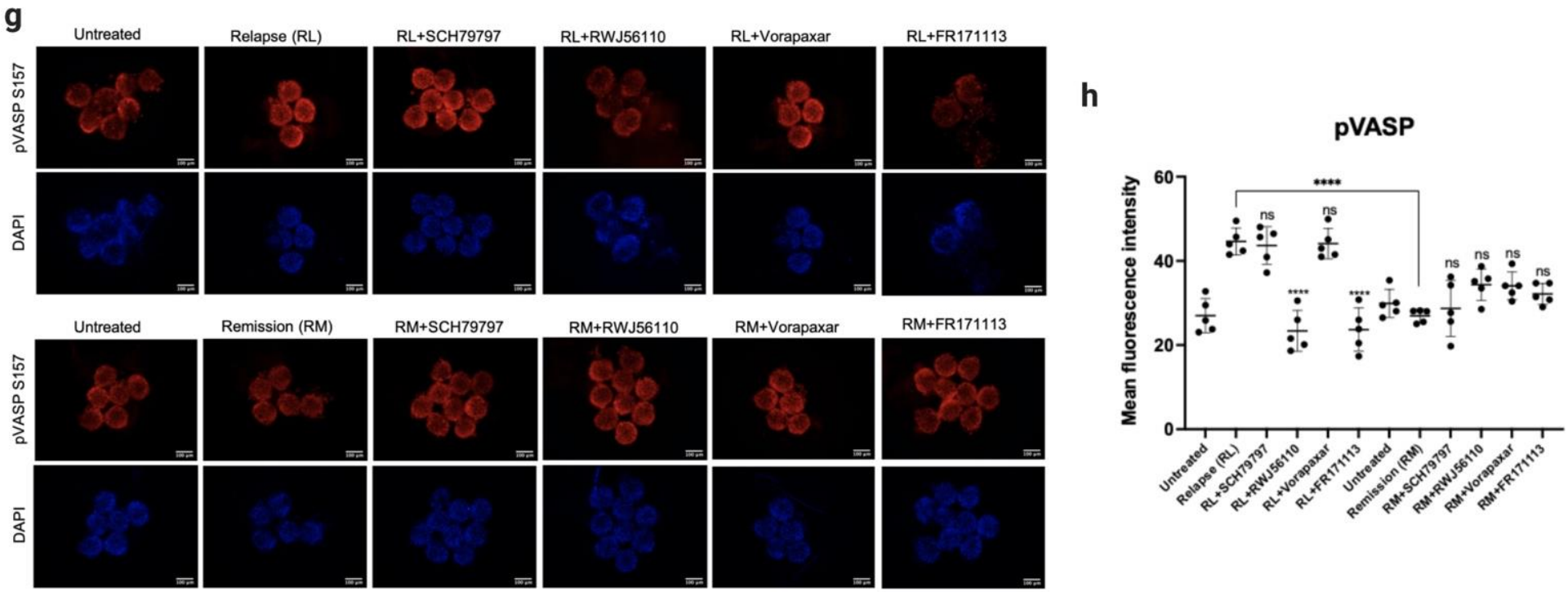

Figure 6

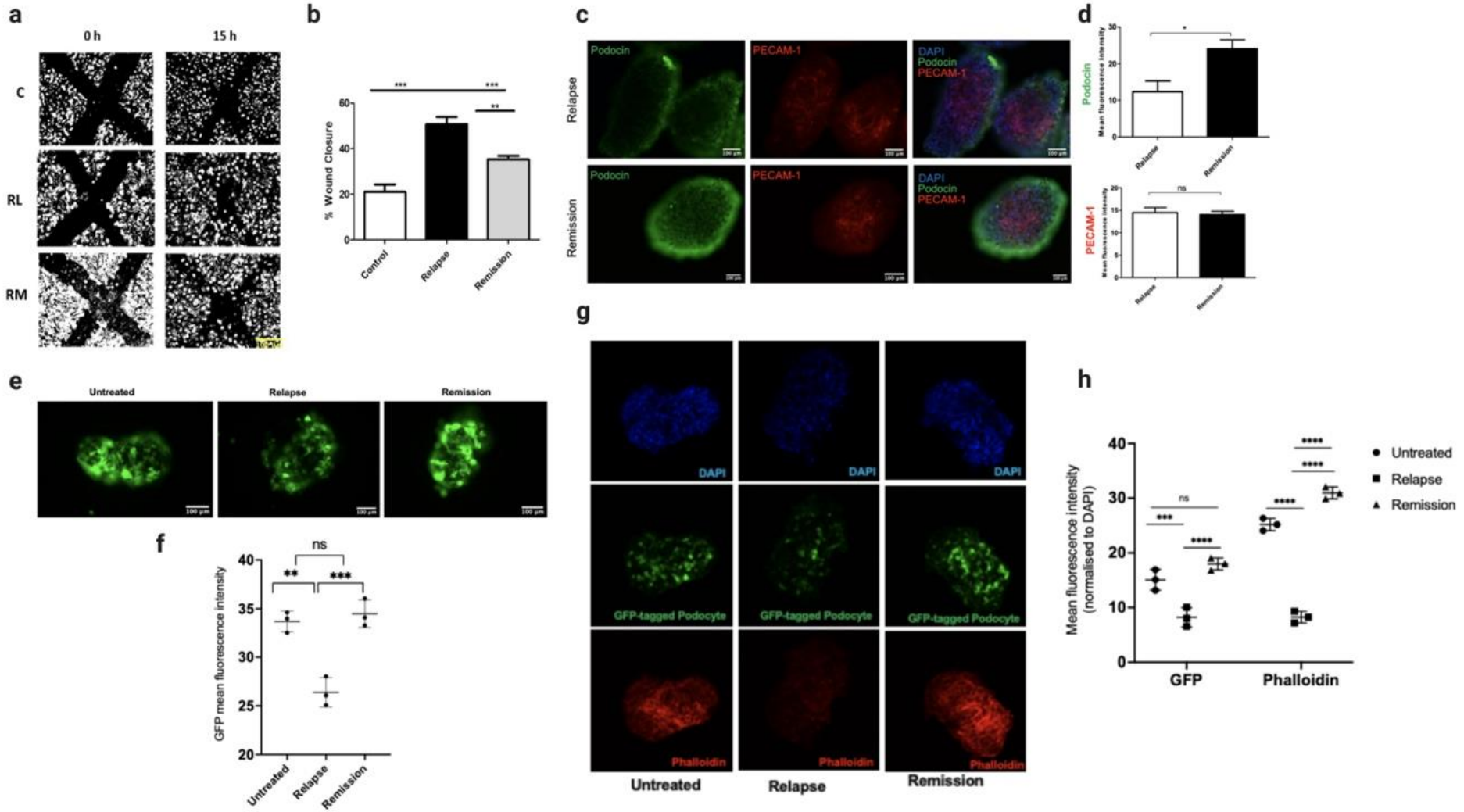
a
0 h
15 h
C
RL
RM
b
% Wound Closure
Control
Relapse
Remission
c
Relapse
Remission
Podocin
PECAM-1
DAPI
d
Podocin
PECAM-1
Mean fluorescence intensity
ns
e
Untreated
Relapse
Remission
f
GFP mean fluorescence intensity
ns
g
DAPI
GFP-tagged Podocyte
Phalloidin
Untreated
Relapse
Remission
h
Mean fluorescence intensity (normalised to DAPI)
GFP
Phalloidin
Untreated
Relapse
Remission

Figure 7

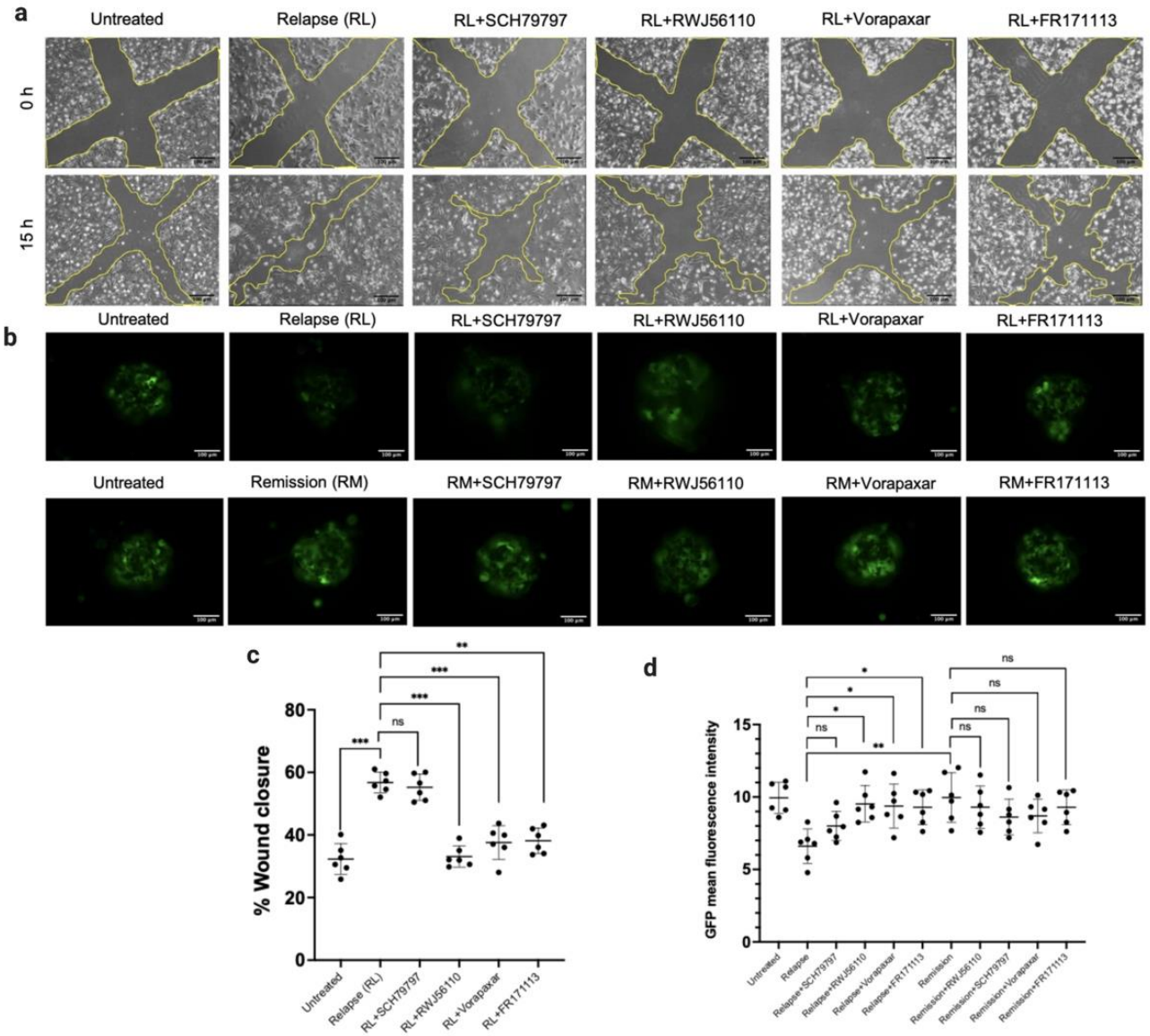
a
Untreated
Relapse (RL)
RL+SCH79797
RL+RWJ56110
RL+Vorapaxar
RL+FR171113
0 h
15 h
b
Untreated
Relapse (RL)
RL+SCH79797
RL+RWJ56110
RL+Vorapaxar
RL+FR171113
Untreated
Remission (RM)
RM+SCH79797
RM+RWJ56110
RM+Vorapaxar
RM+FR171113
c
% Wound closure
0
20
40
60
80
ns
***
**
Untreated
Relapse (RL)
RL+SCH79797
RL+RWJ56110
RL+Vorapaxar
RL+FR171113
d
GFP mean fluorescence intensity
0
5
10
15
ns
*
**
Untreated
Relapse
Relapse+SCH79797
Relapse+RWJ56110
Relapse+Vorapaxar
Relapse+FR171113
Remission
Remission+RWJ56110
Remission+SCH79797
Remission+Vorapaxar
Remission+FR171113

Figure 8

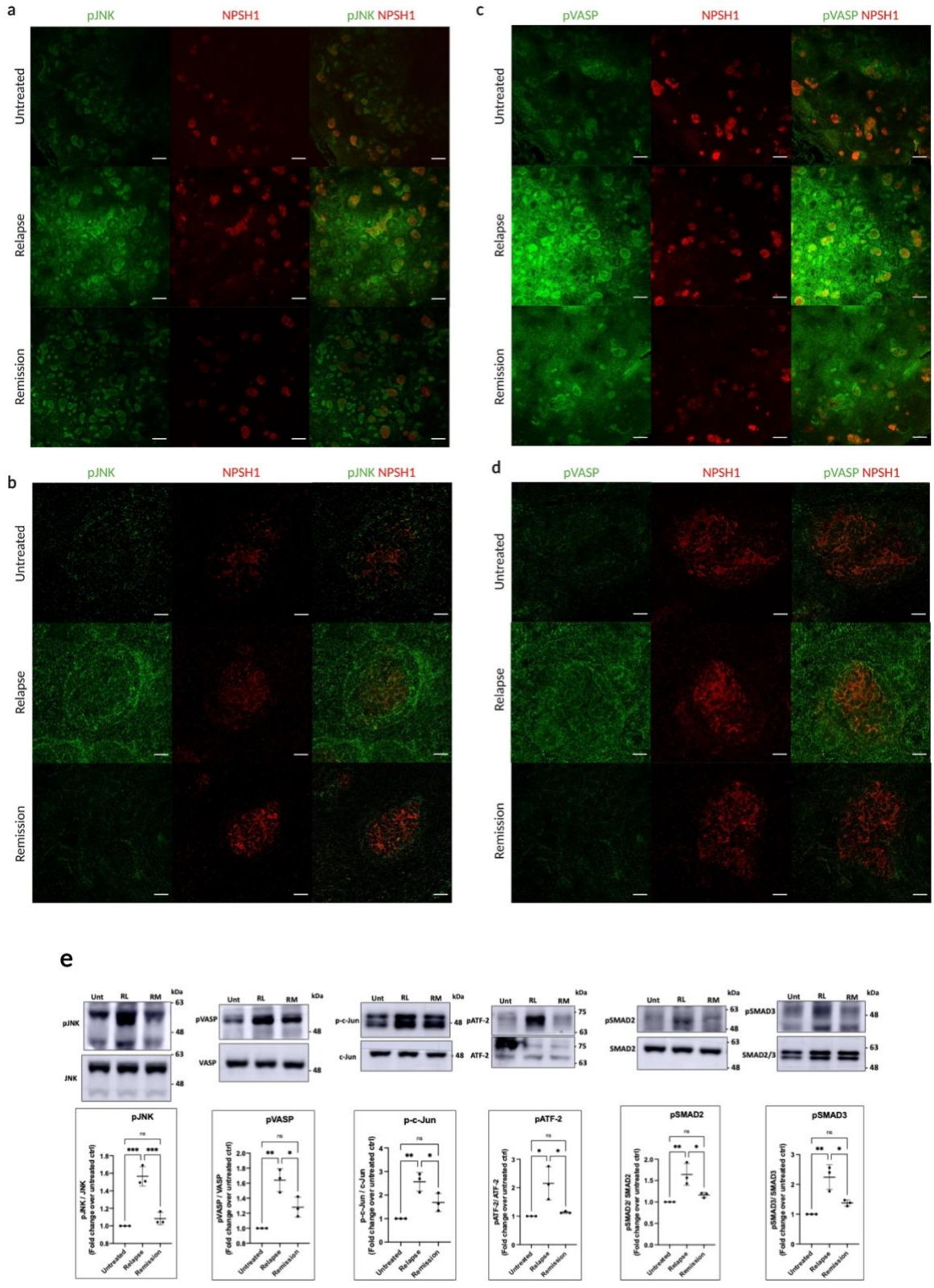
a
pJNK
NPSH1
pJNK NPSH1
Untreated
Relapse
Remission
c
pVASP
NPSH1
pVASP NPSH1
Untreated
Relapse
Remission
b
pJNK
NPSH1
pJNK NPSH1
Untreated
Relapse
Remission
d
pVASP
NPSH1
pVASP NPSH1
Untreated
Relapse
Remission
e
Unt
RL
RM
kDa
pJNK
JNK
pVASP
VASP
p-c-Jun
c-Jun
pATF-2
ATF-2
pSMAD2
SMAD2
pSMAD3
SMAD2/3
pJNK
pVASP
p-c-Jun
pATF-2
pSMAD2
pSMAD3
Untreated
Relapse
Remission

Figure 9

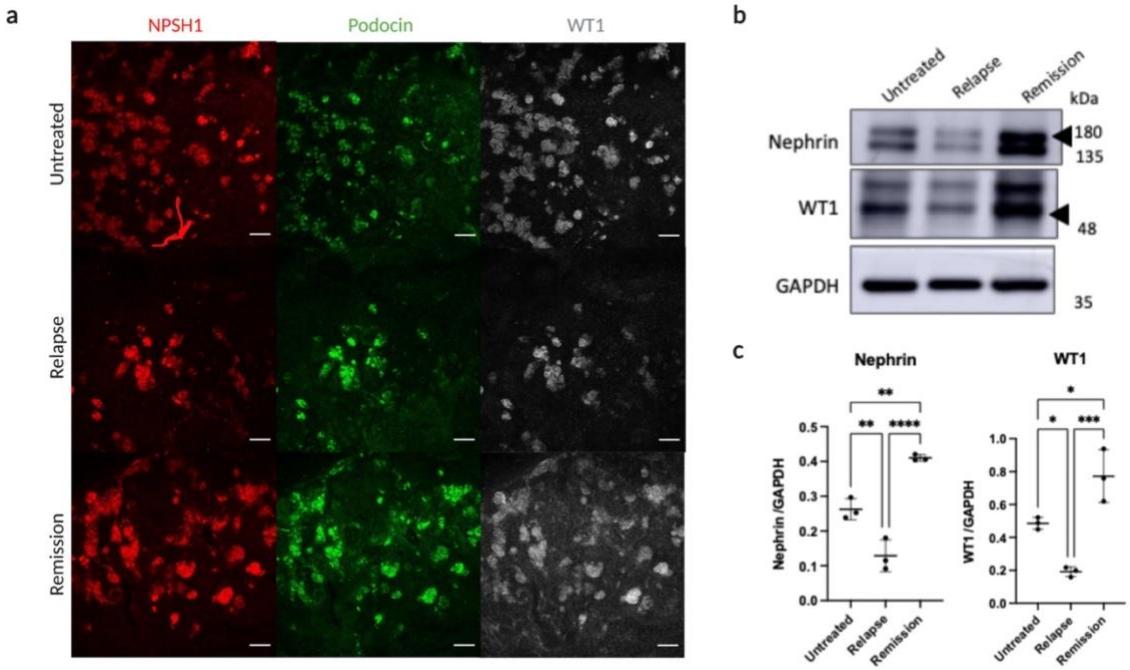

Figure 10

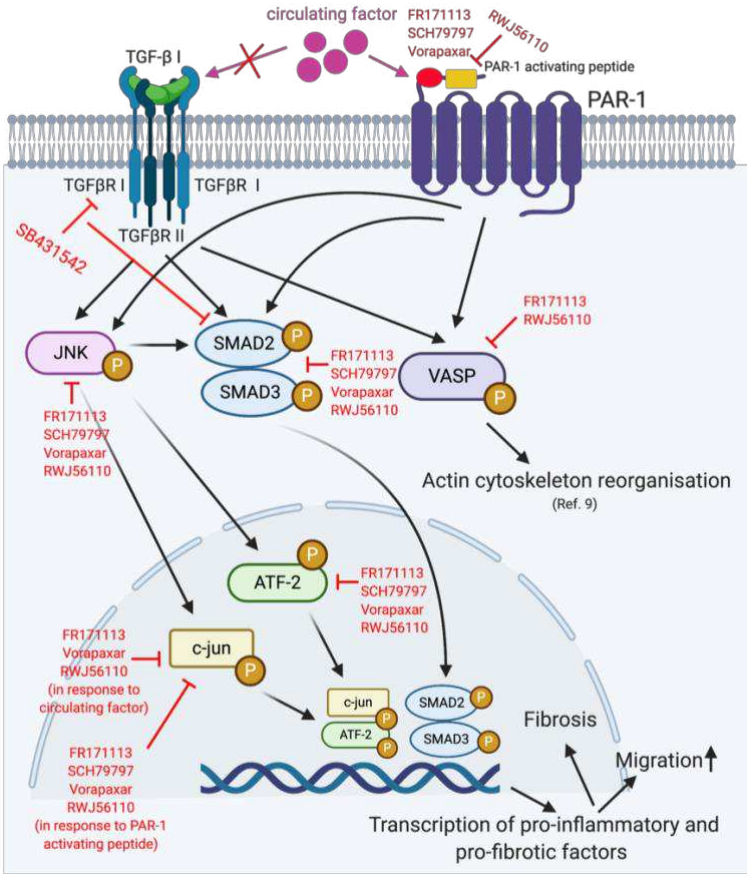

FIGURE LEGENDS

Figure 1: Treatment of podocytes with relapse plasma increases the phosphorylation of JNK, VASP, ATF-2, SMAD3, SMAD2, and c-Jun

Representative blots and semi-quantitative densitometry graphs show the increase phosphorylation of (a) JNK, (b) pVASP S157, (c) ATF-2, (d) SMAD3, (e) SMAD2, and (f) c-Jun in response to SRNS relapse plasma compared to paired remission and untreated control, n=11. * statistically significant with $p<0.05$, ** statistically significant with $p<0.01$, *** statistically significant with $p<0.001$, **** statistically significant with $p<0.0001$; one-way ANOVA, Tukey's Multiple Comparison Test; n=11 different plasma pairs, each experiment performed in triplicate. Results were represented as means ± SD.

Figure 2: Activation of JNK, VASP, ATF-2, c-Jun, SMAD3, and SMAD2 phosphorylation by PAR-1 agonist and TGF-β1 in podocytes

PAR-1 agonist peptide and TGF-β1 stimulate the phosphorylation of JNK, VASP, ATF-2, c-Jun, SMAD3, and SMAD2 in a time-dependent manner. Western blot analysis of phosphorylation of VASP, JNK, ATF-2, c-Jun, SMAD3, and SMAD2 after treatment with 15 μM of PAR-1 agonist (a and b) and TGF-β1 (c and d) for 5, 15, 30, 45, and 60 minutes. * statistically significant with $p<0.05$, ** statistically significant with $p<0.01$, *** statistically significant with $p<0.001$, **** statistically significant with $p<0.0001$ compared with control (untreated); one-way ANOVA, Tukey's Multiple Comparison Test; n=6 different plasma pairs, each experiment performed in triplicate. Data are represented as means ± SD.

Figure 3: Inhibition of nephrotic plasma induced VASP and fibrotic signaling by PAR-1 antagonists

Representative blots (a) and densitometry graphs (b) show that VASP S157, JNK, ATF-2, c-Jun S73, SMAD3, and SMAD2 phosphorylation were significantly increased in response to relapse plasma compared to paired remission and untreated control. These changes were significantly inhibited by PAR-1 antagonists, RWJ56110 and FR171113. SCH79797 and Vorapaxar failed to reduce the phosphorylation of VASP in response to relapse plasma. Also, the phosphorylation of c-Jun at Ser73 was not inhibited in the presence of SCH79797. - = untreated, RL = relapse plasma, RM = remission plasma. $^{\#\#\#\#}$ statistically significant with $p<0.001$ compared with paired-remission plasma treatment * statistically significant with $p<0.05$, ** statistically significant with $p<0.01$, *** statistically significant with $p<0.001$; one-way ANOVA, Tukey's Multiple Comparison Test; n=6 different plasma pairs, each condition performed in triplicate. Results were represented as means ± SD.

Figure 4: SB-43152 does not inhibit SMAD phosphorylation induced by SRNS relapse and remission plasma in podocytes.

ciPods were pre-treated for 30 minutes with 10 and 5 nM of SB-431542 and then induced with relapse and remission plasma for 15 minutes. Western blot (a) and densitometry (b) analysis of the phosphorylation of SMAD3 (pSMAD3/SMAD3), and SMAD2 (pSMAD2/SMAD2). The immunoblots shown are representative blots. RL = Relapse, RM = Remission. * statistically significant with $p<0.05$, ** statistically significant with $p<0.01$, *** statistically significant with $p<0.001$, **** statistically significant with $p<0.0001$; one-way ANOVA, Tukey's Multiple

Comparison Test; n=6 different plasma pairs, each experiment performed in triplicate. Data are represented as means ± SD.

Figure 5: Activation of VASP and JNK on glomerular spheroids by nephrotic plasma
GlomSpheres were treated with relapse and paired-remission plasma at different time points, 5, 15, 30, 45, and 60 minutes. Immunofluorescence stained for phosphor-JNK (a) and phospho-VASP S157 (b) antibodies was performed. Scale bar 100 um. The mean fluorescence intensity of the phosphorylation of JNK (c) began to increase at 15 minutes and peaked at 45 minutes while the phosphorylation of VASP (d) reached the maximum at 15 minutes followed by 30 and 45 minutes after relapse plasma incubation. The signaling to JNK (e and f) was significantly blocked by all four PAR-1 antagonists, while the signaling to VASP (g and h) was significantly inhibited only by RWJ56110 and FR171113. These responses did not occur in remission plasma treatment. Scale bar 100 um. * statistically significant with $p<0.05$, ** statistically significant with $p<0.01$, *** statistically significant with $p<0.001$, **** statistically significant with $p<0.0001$; one-way ANOVA, Tukey's Multiple Comparison Test; t-test for comparing relapse and remission plasma, n=5 different plasma pairs, each experiment performed in triplicate. Data are represented as means ± SD.

Figure 6: Effects of nephrotic plasma on podocyte motility and podocyte loss
(a) Representative images from scratch assay at time 0 h and 15 h. Podocytes treated with relapse plasma were significantly more motile than those treated with paired remission plasma and control (untreated), (n = 7 different plasma pairs); C = control (untreated), RL = relapse plasma, RM = remission plasma. (b) Quantification of the scratch assay. Three independent experiments were performed. (c) Mean fluorescence intensity of glomerular spheroids treated with relapse plasma and remission plasma. (d) Quantification of podocin and PECAM-1 staining for glomerular spheroids across treatment conditions., Treatment of spheroids with relapse plasma significantly reduced podocin fluorescence compared to paired remission * statistically significant with $p=0.0384$, ns=no significance; T-test, n=3 different plasma pairs. (e) Mean fluorescence intensity of GFP podocyte spheroids treated with relapse and paired remission plasma. (f) Quantification of mean GFP fluorescence intensity of podocyte of the spheroids treated with relapse and paired remission plasma. Relapse plasma significantly induced the podocyte loss on spheroids. This effect did not occur to treatment with paired remission plasma. (g) Mean fluorescence intensity of phalloidin and GFP podocyte spheroids treated with relapse and remission plasma. (h) Quantification of mean phalloidin and GFP podocyte fluorescence intensity of the spheroids treated with relapse and paired remission plasma. Results were represented as means ± SD. Scale bar 100 um. ** statistically significant with $p<0.01$, *** statistically significant with $p<0.001$; one-way ANOVA, Tukey's Multiple Comparison Test.

Figure 7: Effects of PAR-1 antagonists on the nephrotic plasma-induced podocyte motility and podocyte loss
PAR-1 antagonists; RWJ56110, Vorapaxar, and FR171113 inhibit relapse plasma-induced podocyte migration in ciPods and podocyte loss in GlomSpheres. (a) Wound size of ciPods after treatment with either relapse plasma or relapse plasma and PAR-1 antagonists for 15 h. (b) Representative images of GFP-tagged podocyte GlomSpheres treated with either relapse plasma, relapse plasma and PAR-1 antagonists, remission plasma, or remission plasma and PAR-1 antagonists. Scale bar 100 um. (c) Quantification of the scratch assay. (d) Quantification

of mean GFP fluorescence intensity of GFP-tagged podocyte in GlomSpheres, n=6 different plasma pairs. Three independent experiments were performed. * statistically significant with p<0.05, ** statistically significant with p<0.01, *** statistically significant with p<0.001, **** statistically significant with p<0.0001; one-way ANOVA, Tukey's Multiple Comparison Test. Data are represented as means ± SD.

Figure 8: Activation within kidney organoids of VASP, JNK, and proteins involved in fibrotic processes by nephrotic plasma

Kidney organoids treated with relapse plasma show the increase in phosphorylation of JNK (a) and VASP (c), specifically in the glomeruli of organoids. Scale bar 100 um. Higher magnification images of the glomeruli of organoids show the co-localization of pJNK and Nephrin (b) and pVASP and Nephrin (d) only in the glomeruli of organoids treated with relapse plasma. Scale bar 25 um. (e) Western blot analysis shows the increase of pVASP, pJNK, pATF-2, pc-Jun, pSMAD2, and pSMAD3 protein levels in organoids in response to relapse plasma. * statistically significant with p<0.05, ** statistically significant with p<0.01, *** statistically significant with p<0.001, **** statistically significant with p<0.0001; one-way ANOVA, Tukey's Multiple Comparison Test. Data are represented as means ± SD.

Figure 9: Effects of nephrotic plasma on podocyte loss in kidney organoids

(a) Immunostaining of kidney organoids show reduced Nephrin, Podocin, and WT1 protein levels in kidney organoids treated with relapse plasma compared to remission and untreated. Scale bar 100 um. (b) Western blot analysis of NEPHRIN and WT1 protein levels confirms the significant decrease of these proteins in organoids treated with relapse plasma. * statistically significant with p<0.05, ** statistically significant with p<0.01, *** statistically significant with p<0.001, **** statistically significant with p<0.0001; one-way ANOVA, Tukey's Multiple Comparison Test. Data are represented as means ± SD.

Figure 10: Proposed mechanism of PAR-1 signaling induced by circulating factor in SRNS

Activation of PAR-1 by circulating factor leads to phosphorylation of JNK in combination with TGF-ß1/SMAD pathway. Activated JNK phosphorylates SMAD2 and SMAD3 via the activation of ATF-2 and c-Jun. Also, the circulating factor could directly activate SMAD2 and SMAD3 which may lead to podocyte injury (fibrosis, podocyte loss, enhanced migration). Alternatively, it may activate VASP leading to actin cytoskeleton reorganization and podocyte motility.

Supplementary Files

This is a list of supplementary files associated with this preprint. Click to download.

- SupplementaryMaterial.pdf